

A Brief Review of Wormhole Cosmic Censorship

Leonel Bixano,^{1,*} I. A. Sarmiento-Alvarado,^{1,†} and Tonatiuh Matos^{1,‡}

¹*Departamento de Física, Centro de Investigación y de Estudios Avanzados del Instituto Politécnico Nacional, Av. Instituto Politécnico Nacional 2508, San Pedro Zacatenco, México 07360, CDMX.*

(Dated: February 19, 2026)

Spacetime singularities, in the sense that curvature invariants are infinite at some point or region, are thought to be impossible to observe, and must be hidden within an event horizon. This conjecture is called Cosmic Censorship (CC), and was formulated by Penrose. Here we review another type of CC where spacetime singularities are causally disconnected from the universe, because the throat of a wormhole “sucks in” the geodesics and prevents them from making contact with the singularity. In this work, we present a series of exact solutions to the Einstein–Maxwell–Dilaton equations that feature a ring singularity; that is, the curvature invariants are singular in this ring, but the ring is causally disconnected from the universe so that no geodesics can touch it. This extension of CC is called Wormhole Cosmic Censorship.

I. INTRODUCTION

Wormholes, explored in general relativity, were first addressed by Ellis and Bronnikov [4, 10], who provided solutions involving scalar fields without event horizons. Morris and Thorne [31] later described traversable wormholes requiring exotic matter. Visser [37] expanded this by developing Lorentzian and “thin-shell” wormholes, reducing the need for exotic matter. Recent research includes the Einstein–Maxwell–Scalar Field theory [12, 17, 19], offering solutions with a phantom scalar field. In this work, we will present one that meets energy conditions without exotic matter (Dilaton scalar field).

On the other hand, spacetime singularities are one of the most intriguing objects we study in general relativity. These singularities are understood as points or regions where some curvature invariant is singular. We believe that these types of singularities must be hidden by some type of physical object to make it impossible to see them and establish causal contact with them, thus preventing any physical violations. In 1964, Penrose in [32] showed that gravitational collapse could create spacetime singularities under certain conditions. Around the same period, Hawking studied cosmological singularities. In 1969, Penrose in [33] suggested that such singularities are hidden by event horizons, forming the basis of the *Cosmic Censorship Conjecture (CCC)*, which was later refined by Hawking and Ellis [13–15]. Penrose’s (CCC) and Matos’s *Wormhole Cosmic Censorship Conjecture* both aim to maintain cosmic causal order by concealing singularities. Penrose’s applies to black holes using event horizons, while Matos’s applies to traversable wormholes using the wormhole’s topology. The WCCC extends the CCC principle to wormhole spacetimes, *applicable across multiple exact solutions and theories*. WCCC ensures that traversable wormholes have singularities that are causally hidden by the wormhole structure. This makes wormholes safer and more physically possible, allowing traversal without encountering singularities. We demonstrate that certain precise solutions of Einstein’s field equations, which exhibit spacetime singularities, possess a common attribute: the singularities remain unobservable as the wormhole absorbs the geodesics, thereby inhibiting the spacetime singularity from establishing causal interaction with the universe. We conduct a re-examination of some of these exact solutions and establish that they are, indeed, causally isolated from the universe.

Visser and Poisson [34] describe a “cut and paste” method for thin-shell wormholes and assess their stability. Lobo [19] examines the use of phantom energy to support throats, highlighting necessary violations of the NEC in regular geometries. Gao, Jafferis, and Wall [11] make AdS wormholes traversable via a quantum mechanism involving negative average null energy. Maldacena, Milekhin, and Popov [22] maintain a wormhole in asymptotically flat 4D using Casimir energy, resulting in a large smooth throat without causal violations. Altogether, thin-shell (classical), phantom (classical with NEC ≤ 0), and semiclassical/AdS-CFT wormholes achieve traversability without visible singularities, which places the WCCC well in the modern landscape. When a singularity exists (e.g., ring in rotating solutions), it must remain causally untouchable. If singularities does not exist (previous cases), consistency is immediate, and *there is no reason for censoring singularities*.

We start by examining the Einstein–Maxwell Lagrangian coupled to a dilaton or ghost scalar field. Notable theories studied in this work include Einstein–Maxwell theories with an uncoupled scalar field, low-energy superstrings (S-S),

* Contact author: leonel.delacruz@cinvestav.mx

† Contact author: ignacio.sarmiento@cinvestav.mx

‡ Contact author: tonatiuh.matos@cinvestav.mx

Kaluza–Klein (K-K), or Entanglement Relativity (E-R). Thus, we start with the Lagrangian

$$\mathcal{L} = \sqrt{-g} \left(-\frac{1}{\mu_0 \sigma_0} R + \frac{1}{\mu_0 \sigma_0} 2\epsilon_0 (\nabla\phi)^2 + \frac{1}{\mu_0} e^{-2\alpha_0\phi} F^2 \right), \quad (1)$$

where $\sigma_0 = 8\pi G/(\mu_0 c^4)$, c represents the speed of light, G denotes the gravitational constant, and μ_0 is the vacuum permeability, R is Ricci scalar, ϕ is scalar field, and F^2 is invariant generated by the Faraday tensor. Here the constant ϵ_0 can only take two values—1 if ϕ is a dilatonic scalar field and -1 if it is a ghost scalar field—while the constant α_0 defines the theory in question. Prominent theories in this field include $\alpha_0^2 = 0, 1, 3$, corresponding to the Einstein–Maxwell theories with an uncoupled scalar field, low-energy S-S, and K-K theories. Notably, this formulation also encapsulates emerging theories, such as the E-R (applications of this theory can be found in [28–30]) where $\alpha_0^2 = 1/12$.

Employing variational methods to derive the associated field equations, we obtain the following:

$$\nabla_\mu (e^{-2\alpha_0\phi} F^{\mu\nu}) = 0, \quad (2a)$$

$$\epsilon_0 \nabla^2 \phi + \frac{\alpha_0}{2} \sigma_0 (e^{-2\alpha_0\phi} F^2) = 0, \quad (2b)$$

$$R_{\mu\nu} = 2\epsilon_0 \nabla_\mu \phi \nabla_\nu \phi + 2\sigma_0 e^{-2\alpha_0\phi} \left(F_{\mu\sigma} F_\nu{}^\sigma - \frac{1}{4} g_{\mu\nu} F^2 \right), \quad (2c)$$

In the Section II, we will present the symmetries considered of the spacetime, and the solutions, alongside their respective behavior of the metric function and the equations for the constraint parameters.

The Section III will address the comprehensive physical analysis of solution (11), which encompasses all relevant information from solutions (8) and (9).

The Section IV provides the Penrose diagram and the causal structure, thereby demonstrating the validity of these solutions and their global hyperbolicity.

In Section V, we will introduce an analogous method for obtaining new solutions in higher dimensions, utilizing $\alpha_0^2 = 3$, i.e., within the framework of Kaluza–Klein Theories.

Lastly, we will present a novel solution utilizing the methodology outlined in Section V, which is currently under study.

In this paper, \mathbf{M}_n denotes the set of all $n \times n$ real matrices, and the set of symmetric matrices is denoted by \mathbf{Sym}_n . The centralizer of a subset $\mathcal{A} \subset \mathbf{M}_n$, denoted by $\mathcal{C}(\mathcal{A})$, is defined as $\mathcal{C}(\mathcal{A}) = \{M \in \mathbf{M}_n : MA = AM \text{ for all } A \in \mathcal{A}\}$.

II. ANALYSED SOLUTIONS

To solve field Equation (2), we employed a stationary and axially symmetric spacetime, characterized by the existence of two Killing vectors $\{\partial_t, \partial_\varphi\}$. In Weyl ($\rho = \sqrt{(x^2 + 1)(1 - y^2)}$, $z = Lxy$), and spheroidal ($Lx = r - l_1$, $y = \cos\theta$) (where (r, θ) corresponds to Boyer–Lindquist coordinates) coordinate systems, the metric is successively represented by the following forms:

$$ds^2 = -f \{d(ct) - \omega d\varphi\}^2 + f^{-1} \{e^{2k}(d\rho^2 + dz^2) + \rho^2 d\varphi^2\} \quad (3a)$$

$$= -f (d(ct) - \omega d\varphi)^2 + f^{-1} \left(L^2(x^2 + 1)(1 - y^2) d\varphi^2 + L^2(x^2 + y^2) e^{2k} \left\{ \frac{dx^2}{x^2 + 1} + \frac{dy^2}{1 - y^2} \right\} \right), \quad (3b)$$

where $\rho \in [0, \infty)$, $\{z, x\} \in \mathbb{R}$, $y \in [-1, 1]$, $\theta \in [0, \pi]$, and $r \in (-\infty, -l_1] \cup [l_1, \infty)$.

In the same way, considering these symmetries, we can use the following ansatz for the electromagnetic 4-potential:

$$A_\mu = \left[A_t(\rho, z), 0, 0, A_\varphi(\rho, z) \right]. \quad (4)$$

The family utilized to derive novel solutions is *second class of solutions*:

$$f = f_0, \quad \kappa = \kappa_0 e^\lambda, \quad \psi = \frac{\sqrt{f_0}}{\sqrt{\sigma_0 \kappa_0}} e^{-\lambda} + \psi_0, \quad \chi = \sqrt{\sigma_0} \sqrt{f_0 \kappa_0} e^\lambda + \chi_0, \quad \epsilon = b_0, \quad (5)$$

in which $\{f_0, \psi_0, \chi_0, \kappa_0, b_0\}$ represent the integration constants, $(f, \epsilon, \psi, \chi, \kappa)$ denote the gravitational, rotational, electric, magnetic, and scalar potentials analogous to Ernst potentials, and $\lambda(x, y)$ constitutes a general coordinate of a two-dimensional subspace that facilitates the solution of the field equations satisfying the Laplace equation.

$$\partial_x \{(x^2 + 1)\partial_x \lambda\} + \partial_y \{(1 - y^2)\partial_y \lambda\} = 0. \quad (6)$$

A comprehensive calculation and explanation to derive the corresponding family of solutions and beyond is provided in [23, 25].

In [26], two solutions to (6) were introduced, referred to as λ_5, λ_6 :

$$\lambda_5 = \lambda_0 \frac{x}{(x^2 + y^2)}, \quad (7a)$$

$$\lambda_6 = \lambda_0 \frac{y}{(x^2 + y^2)}, \quad (7b)$$

where λ_0 is a integration constant.

A. Solution 5

In [1], the electromagnetic 4-potential and metric functions associated with λ_5 were derived and analyzed, and are presented in the subsequent expressions:

$$f = f_0 = 1, \quad (8a)$$

$$\omega_5 = -L \frac{\lambda_0}{f_0} \left(\frac{y(x^2 + 1)}{x^2 + y^2} \right), \quad (8b)$$

$$A_{\varphi 5} = -\frac{\sqrt{f_0}}{2\kappa_0 \sqrt{\sigma_0}} \frac{\omega_5}{L} e^{-\lambda_5}, \quad (8c)$$

$$A_{t5} = \frac{\sqrt{f_0}}{2\kappa_0 \sqrt{\sigma_0}} e^{-\lambda_5}, \quad (8d)$$

$$k_{\lambda_5} = -k_0 \lambda_0^2 \frac{(1 - y^2)}{4(x^2 + y^2)^4} \left(-8x^2 y^2 (x^2 + 1) + (x^2 + y^2)^2 \{(1 - y^2) + 2(x^2 + y^2)\} \right), \quad (8e)$$

where k_0 is a integration constant corresponding to the function metric $k(x, y)$.

B. Solution 6

The subsequent expressions present the electromagnetic 4-potential and metric functions related to λ_6 , which were derived and examined in [8].

$$f = f_0 = 1, \quad (9a)$$

$$\omega_6 = \frac{L\lambda_0}{f_0} \frac{x(1 - y^2)}{x^2 + y^2}, \quad (9b)$$

$$A_{\varphi 6} = -\frac{\sqrt{f_0}}{2\kappa_0 \sqrt{\sigma_0}} \frac{\omega_6}{L} e^{-\lambda_6}, \quad (9c)$$

$$A_{t6} = \frac{\sqrt{f_0}}{2\kappa_0 \sqrt{\sigma_0}} e^{-\lambda_6} \quad (9d)$$

$$k_{\lambda_6} = -k_0 \lambda_0^2 \frac{(1 - y^2)}{4(x^2 + y^2)^4} \left(8x^2 y^2 (x^2 + 1) - (x^2 + y^2)^2 (1 - y^2) \right). \quad (9e)$$

C. Combination Solution

Moreover, Bixano and Matos [2] analyzed the combination of (8) and (9), and using this combination, we can encompass both previously mentioned solutions.

It is important to note that, while the combination of the solutions is linear as per term λ

$$\lambda_c = \frac{\lambda_0 y + \tau_0 x}{(x^2 + y^2)}, \quad (10)$$

the function metrics themselves are not. This is due to the necessity of resolving more complicate equations, as elaborated in [1, 2, 8, 25, 26].

For the combination solution, the functions metric and the electromagnetic 4-potential are

$$f = f_0 = 1, \quad (11a)$$

$$\omega = \frac{L}{f_0} \left(\frac{\lambda_0 x(1 - y^2) - \tau_0 y(x^2 + 1)}{x^2 + y^2} \right), \quad (11b)$$

$$A_\varphi = \frac{\sqrt{f_0}}{2\kappa_0 \sqrt{\sigma_0}} \left(A_3 - \frac{\omega}{L} e^{-\lambda_c} \right), \quad (11c)$$

$$A_t = \frac{\sqrt{f_0}}{2\kappa_0 \sqrt{\sigma_0}} \left(e^{-\lambda_c} - 1 \right) \quad (11d)$$

$$k_c = k_{\lambda_5} + k_{\lambda_6} - k_0 \frac{8xy(1 - y^2)(x^2 + 1)(x^2 - y^2)\lambda_0\tau_0}{4(x^2 + y^2)^4}, \quad (11e)$$

For our objective, it is imperative to consider the asymptotic behavior of (11)

$$\lim_{x \rightarrow \pm\infty} \omega(x, y) = -\tau_0 L y, \quad (12a)$$

$$\omega(0, y) = -\frac{\tau_0 L}{y}, \quad (12b)$$

$$\omega(x, 0) = \frac{L\lambda_0}{x}, \quad (12c)$$

$$\omega(x, 1) = -L\tau_0, \quad (12d)$$

$$\text{For } x \gg 1 \text{ we have } k_c \approx -k_0 \tau_0^2 \frac{(1 - y^2)}{2x^2}, \quad (13a)$$

$$k_c(0, y) = \frac{k_0(1 - y^2)}{4y^4} \{ \lambda_0^2(1 - y^2) - \tau_0^2(1 + y^2) \}, \quad (13b)$$

$$k_c(x, 0) = k_0 \frac{(\lambda_0^2 - \tau_0^2(2x^2 + 1))}{4x^4}, \quad (13c)$$

$$k_c(x, 1) = 0. \quad (13d)$$

Using the solution provided in (11), which encapsulates all pertinent information related to (8) and (9), we shall exclusively include the Ricci scalar, Kretschmann scalar, and the difference between density and pressure (this expression is in the comoving frame, i.e., in the diagonal tetrad. For additional details, refer to [1, 2, 8, 31]) pertaining to (11).

$$R = \frac{(4k_0 + 1)e^{-2k_c}}{2L^2(x^2 + y^2)^4} \left\{ \lambda_0^2 \left(y^2(1 - y^2) + x^2(3y^2 + 1) \right) + \tau_0^2 \left(y^2 + x^2(x^2 - 3y^2 + 1) \right) + 4\lambda_0\tau_0 xy(x^2 - y^2) \right\}, \quad (14a)$$

$$KN = \frac{F_c(x, y)}{8L^4(x^2 + y^2)^{12}} e^{-4k(x, y)}, \quad (14b)$$

$$\varrho - P = \frac{e^{-2k_c}}{2L^2(x^2 + y^2)^5} \left\{ 4\lambda_0\tau_0 xy(x^2 - y^2) \left(x^2 + 2y^2 - 1 + 4k_0(x^2 + 1) \right) + 2\lambda_0^2 \left(y^4(1 - y^2) + x^4(1 + (1 + 8k_0)y^2) \right) \right. \\ \left. + 2(4k_0 + y^2)x^2y^2 \right\} + \tau_0^2 \left[(4k_0 + 1)(x^2 + 1)x^4 - 2x^2y^2(4k_0(x^2 + 1) + x^2 - 3) + (1 + 4k_0 + (4k_0 - 7)x^2)y^4 \right], \quad (15)$$

wherein $F_c(x, y)$ denotes a polynomial whose degree is inferior to $(x^2 + y^2)^{12}$.

D. Constraint Parameters

Substituting the solution (11) associated with λ_c , and the scalar field

$$\phi(x, y) = -\frac{\lambda_c}{\alpha_0}, \quad (16)$$

in (2), the constraint on the free parameters of the solution is

$$\alpha_0^2(4k_0 + 1) - 4\epsilon_0 = 0. \quad (17)$$

Table I summarises the results.

Upon careful consideration of (17), it becomes evident that $(4k_0 + 1) = 4\epsilon_0/\alpha_0^2$, then

$$\begin{aligned} \text{if we have a Dilatonic field } (\epsilon = 1) &\Rightarrow (4k_0 + 1) > 0, \\ \text{if we have a Phantom field } (\epsilon = -1) &\Rightarrow (4k_0 + 1) < 0. \end{aligned}$$

III. PHYSICAL ANALYSIS

In this study, we present solely the most significant result. For an in-depth exploration of the calculations, readers are referred to the detailed expositions in the papers [1–3, 8].

A. Singularities and Asymptotical Flatness

By employing Equations (14a) and (14b), it is evident that a singularity exists at the point $x = y = 0$, which is represented by *ring singularity* $r = l_1$ and $\theta = \pi/2$ within the framework of Lewis–Papapetrou coordinates, or alternatively by $\rho = L$ and $z = 0$ in the context of Weyl coordinates.

It is now understood that this singularity is causally disconnected; however, the numerical analysis provided in [2, 6, 27] lays the groundwork for the early progress of the WCC. Subsequently, in [3, 7], this conjecture, analogous to the Cosmic Censorship proposed by Penrose [33] and further refined by Hawking and Ellis [16], is demonstrated analytically.

Conversely, considering the limit as $r \rightarrow \pm\infty \Rightarrow x \rightarrow \pm\infty$, it becomes evident that both (14a) and (14b) converge to 0, irrespective of the sign of $(4k_0 + 1)$. This indicates that the nature of a dilatonic or phantom scalar field is not important in terms of asymptotic behaviour. The solution (11) presented in this work is *asymptotically flat when we fix* $\tau_0 = 0$; consequently, the solution analyzed in [8] is the only one possessing physical significance; however, this does not imply that the combined solution lacks importance.

B. Null Energy Conditions

The characteristics of the expression (15) are examined across various regions as follows:

$$\text{For } x \gg 1 \text{ implies } (\varrho - P) \approx \frac{(4k_0 + 1)\tau_0^2}{2L^2x^4}, \quad (18a)$$

TABLE I: Values of k_0 .

α_0^2	Dilatonic Field ($\epsilon_0 = 1$)	Phantom Field ($\epsilon_0 = -1$)
1/12	47/4	-49/4
1	3/4	-5/4
3	1/12	-7/12
4	0	-1/2
$n \geq 5$	$(4 - n)/4n$	$-(4 + n)/n$

$$\lim_{x \rightarrow 0} (\varrho - P) = \frac{e^{-2k_c(0,y)}}{2L^2 y^6} \left\{ 2\lambda_0^2(1-y^2) + \tau_0^2(4k_0+1) \right\}, \quad (18b)$$

$$\lim_{x \rightarrow y} (\varrho - P) = \frac{e^{-2k_c(y,y)}}{16L^2 y^6} \left\{ 2\tau_0^2(1-y^2) + \lambda_0^2(4k_0+1)(1+y^2) \right\}, \quad (18c)$$

$$(\varrho - P)|_{y=0} = \frac{e^{-2k_c(x,0)}}{2L^2 x^6} \left\{ 2\lambda_0^2 + \tau_0^2(4k_0+1)(x^2+1) \right\}, \quad (18d)$$

$$(\varrho - P)|_{y=1} = (4k_0+1) \frac{(2\lambda_0 x + \tau_0 \{x^2 - 1\})^2}{2L^2 (x^2 + 1)^4}. \quad (18e)$$

Upon conducting a thorough analysis of all the equations presented in (18), three significant observations can be discerned:

- All the possible values of an exponential function is $e^k \in [0, \infty)$.
- Given $y \in [-1, 1]$ and subsequently $y^{2n} \in [0, 1]$, this implies that $(1 - y^2) > 0$.
- The terms of λ_0, τ_0, x, y with even exponents yield solely positive values.

Therefore, the crucial factor determining the fulfillment of the NEC is $(4k_0 + 1)$. In other words

$$\begin{aligned} \text{Dilatonic Field} & \quad \text{implies} \quad (\varrho - P) > 0, \\ \text{Phantom Field} & \quad \text{implies} \quad (\varrho - P) < 0. \end{aligned}$$

C. Geometries

To determine the profile of the compact object or the form of the wormhole's throat, it is necessary to initially select a hypersurface with constants t and y of (3), and subsequently embed it into a cylindrical plane space (for more details on the method, see [2, 7, 20]).

The differential equations of the embedded diagrams, which were solved using numerical methods with the initial condition $z(0) = 0$ and parameters $\lambda_0 = 10^{-2}$, $\tau_0 = 10^{-3}$, $k_0 = 1/12$, $L = 1$ km, are

$$\bar{\rho}(x, y_0)^2 = L^2(x^2 + 1)(1 - y_0^2) - \omega(x, y_0)^2, \quad (19a)$$

$$\left(\frac{d\bar{\rho}}{dx} \right)^2 + \left(\frac{dz}{dx} \right)^2 = L^2 \frac{(x^2 + y_0^2)}{x^2 + 1} e^{2k(x, y_0)}. \quad (19b)$$

$$\bar{\rho}(x_0, y)^2 = L^2(x_0^2 + 1)(1 - y^2) - \omega(x_0, y)^2, \quad (20a)$$

$$\left(\frac{d\bar{\rho}}{dy} \right)^2 + \left(\frac{dz}{dy} \right)^2 = L^2 \frac{(x_0^2 + y^2)}{1 - y^2} e^{2k(x_0, y)}. \quad (20b)$$

The embedded diagrams can be viewed in Figure 1. The black dashed lines in Figure 1a,b represent the size of the wormhole's throat, while each colored line corresponds to a specific profile or shape defined by y_0 and x_0 , respectively. In the case of Figure 1a, $z > 0$ corresponds to one universe, $z < 0$ corresponds to another universe or possibly the same universe at different coordinates, and $z(0) = 0$ denotes the throat. The initial two figures of Figure 1 indicate that traversing a wormhole along the polar axis results in a closure of the throat, thereby demonstrating that the wormhole is effectively closed in this direction, while presenting its maximum dimension within the equatorial plane. (These assumptions are valid for (8), (9), and (11).)

This embedding technique demonstrates the dependency of the throat size on the angle, specifically, the function

$$\rho(x, y) = L\sqrt{(x^2 + 1)(1 - y^2)} = \sqrt{(r - l_1)^2 + L^2} \sin \theta, \quad (21)$$

represents an effective radial function for wormholes that lack spherical symmetry (independence of θ).

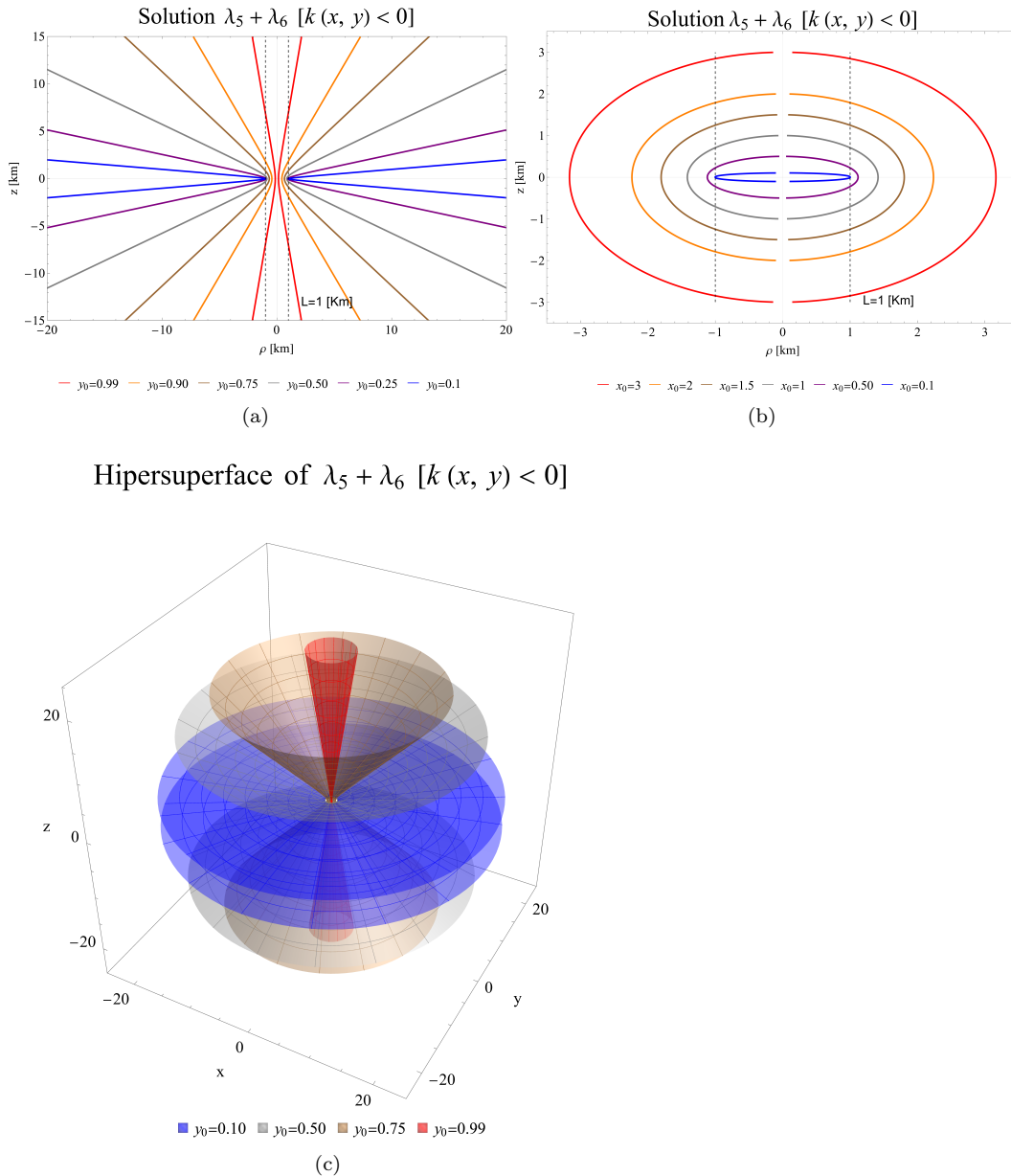


FIG. 1: All units in the graphs are expressed in kilometers and were taken from [2]. Embedding diagrams corresponding to solution (11): (a) Wormhole profile. (b) Throat shape. (c) Revolution surface of the wormhole profile.

D. Tidal Forces

To examine tidal forces, we can employ the methodology outlined in [31], as utilized in [1, 2, 8]. This approach leverages a transformation from the comoving frame to an astronaut frame to analyze the geodesic deviation equation. The transformation provides the following representation of the aforementioned equation:

$$|R_{\hat{\mu} \hat{0} \hat{\mu} \hat{0}}| \leq \frac{g_{Earth}}{2m * c^2} \approx (10^5 \text{Km})^{-2}. \quad (22)$$

where the subscript $\hat{\mu}$ denotes the component of the Ricci tensor within the astronaut's reference frame.

The results provide a comprehensive understanding of this class of wormholes (5). The most secure method for traversing the wormhole is in proximity to the polar axis, although not precisely along it. Near the equatorial

plane, traversal is not feasible due to the presence of exceedingly hazardous regions, particularly when considering components $R_{\hat{\mu} \hat{0} \hat{\mu} \hat{0}}$ and $\hat{\mu} = 1, 3$.

Considering the tidal forces, a wormhole that optimizes safety possesses a size of

$$L \geq 10^3 \text{ km} \quad \text{which implies that} \quad M_{WH} \geq 10^3 M_{\odot}, \quad (23)$$

where M_{\odot} is a *solar mass*.

E. Geodesics

The geodesics of these wormholes were derived using the Hamiltonian formulation, wherein the corresponding Hamiltonian is as follows:

$$2\mathcal{H} = \frac{f(l_z - \omega E)^2}{L^2(x^2 + 1)(1 - y^2)} - \frac{E^2}{f} + \frac{f e^{-2k}}{L^2(x^2 + y^2)} \left\{ (x^2 + 1)p_x^2 + (1 - y^2)p_y^2 \right\}, \quad (24)$$

where the motion constants are

$$-p_t = E = f(ct - \omega\dot{\varphi}), \quad (25a)$$

$$p_{\varphi} = l_z = \frac{L^2(x^2 + 1)(1 - y^2)}{f} \dot{\varphi} + \omega E, \quad (25b)$$

and the other momenta are

$$p_x = \frac{L^2(x^2 + y^2)e^{2k}}{f(x^2 + 1)} \dot{x}, \quad (26a)$$

$$p_y = \frac{L^2(x^2 + y^2)e^{2k}}{f(1 - y^2)} \dot{y}. \quad (26b)$$

From (25), it is possible to compute the proper angular momentum

$$\frac{\dot{\varphi}}{t} = \frac{d\varphi}{dt} = \frac{f^2(l_z - \omega E)c}{L^2(x^2 + 1)(1 - y^2)E + f^2\omega(l_z - \omega E)}. \quad (27)$$

Thus, employing the following initial values corresponding to a null geodesic,

$$l_z = 1, \quad E = 2, \quad x(0) = 25, \quad p_x(0) = -2, \quad p_y(0) = 0, \quad (28)$$

and arbitrary $y(0) = y_0$, it is feasible to compute the equation of motion numerically

$$\dot{x}^{\mu} \equiv \frac{\partial \mathcal{H}}{\partial p_{\mu}}, \quad \dot{p}_{\mu} \equiv -\frac{\partial \mathcal{H}}{\partial x^{\mu}}. \quad (29)$$

and extend the solution into pseudo-Cartesian coordinate space

$$X_c = \rho \cos\left(\frac{d\varphi}{dt}t\right), \quad Y_c = \rho \sin\left(\frac{d\varphi}{dt}t\right), \quad Z_c = z. \quad (30)$$

The parameters used were $\lambda_0 = 10^{-2}$, $\tau_0 = 10^{-3}$, $k_0 = 1/12$, and a sun size WH

$$M = M_{\odot} \approx 2 \times 10^{30} \text{ kg}, \quad (31a)$$

$$L < 2l_1 = r_s^{Sun} \approx 3 \times 10^3 \text{ m}. \quad (31b)$$

Figure 2a illustrates the plotted null geodesics corresponding to various values of y_0 within spheroidal coordinates. Positive instances of x are indicative of one universe, whereas negative instances of x are associated either with a separate universe or with the same universe, but in a different spatial domain.

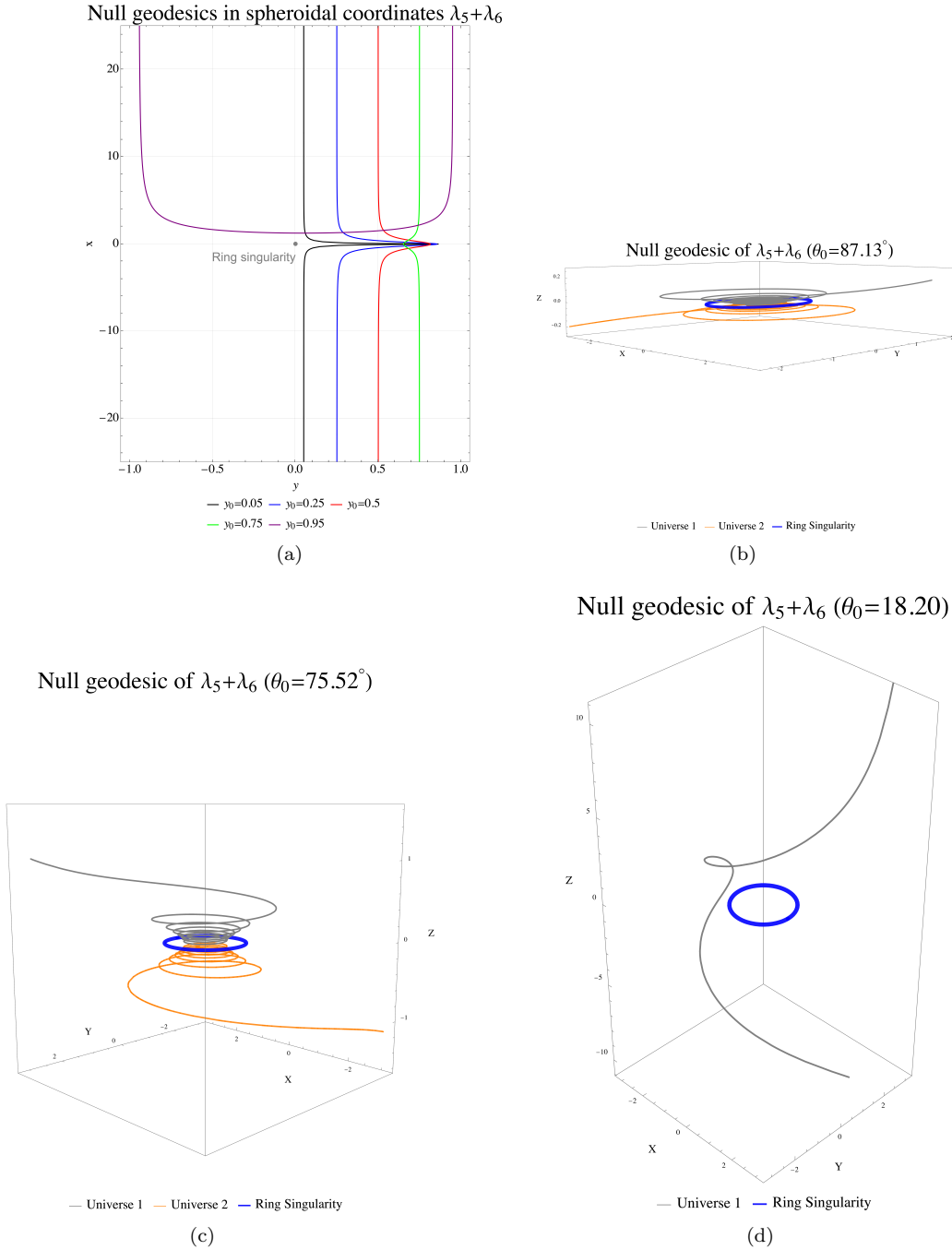


FIG. 2: This illustration is sourced from [2]. (a) This graph depicts null geodesics with varying initial values for y using spheroidal coordinates, where $x > 0$ represents one universe and $x < 0$ signifies another. (b), (c), and (d) illustrate null geodesics in pseudo-Cartesian coordinates, the blue torus symbolizes the ring singularity, the orange colour denotes one universe, and the gray colour signifies another universe.

The remaining three figures in Figure 2 illustrate various null geodesics represented in pseudo-Cartesian coordinates as described in (30). Universe 1 is denoted in gray, while Universe 2 is represented in orange. The ring singularity is depicted as a blue torus. As demonstrated in Figure 2a,d, the geodesic with an initial value of $y_0 = 0.95$ was unable to traverse the wormhole and only approached it.

F. Vectorial Electromagnetic Field

A crucial and intriguing topic of examination is the structure of the vectorial electromagnetic field. Utilizing the representation of the electromagnetic field in Weyl coordinates, as provided by

$$\begin{bmatrix} B_z \\ -B_\rho \end{bmatrix} = \frac{-1/\sqrt{\sigma_0}}{L(x^2 + y^2)} \frac{\sqrt{f_0}}{2\kappa_0} \begin{bmatrix} x\sqrt{(x^2 + 1)(1 - y^2)} & -y\sqrt{(x^2 + 1)(1 - y^2)} \\ y(x^2 + 1) & x(1 - y^2) \end{bmatrix} \begin{bmatrix} \partial_x \\ \partial_y \end{bmatrix} \left(\frac{\omega}{L} e^{-\lambda_c} \right), \quad (32a)$$

$$\begin{bmatrix} E_\rho \\ E_z \end{bmatrix} = \frac{c/\sqrt{\sigma_0}}{L(x^2 + y^2)} \frac{\sqrt{f_0}}{2\kappa_0} \begin{bmatrix} x\sqrt{(x^2 + 1)(1 - y^2)} & -y\sqrt{(x^2 + 1)(1 - y^2)} \\ y(x^2 + 1) & x(1 - y^2) \end{bmatrix} \begin{bmatrix} \partial_x \\ \partial_y \end{bmatrix} (e^{-\lambda_c}), \quad (32b)$$

we are able to visualize the vectorial field. However, in this instance, it is necessary to employ pseudo-Cartesian coordinates once more. For this purpose, the electromagnetic field will be projected in each direction (u, v, w) provided by

$$\begin{aligned} H_u(u, v, w) &= H_\rho(u, v, w) \cos\left(\frac{d\varphi}{dt}t\right), \\ H_v(u, v, w) &= H_\rho(u, v, w) \sin\left(\frac{d\varphi}{dt}t\right), \\ H_w(u, v, w) &= H_z(u, v, w), \end{aligned}$$

where the Boyer–Lindquist coordinates are mapped to these pseudo-Cartesian coordinates as follows:

$$Lx + l_1 = r = \sqrt{u^2 + v^2 + w^2}, \quad y = \cos\theta = w/r,$$

The equatorial plane $y = 0$ is in alignment with plane $w = 0$, signifying the presence of a ring singularity at points $w = 0$ and $l_1^2 = u^2 + v^2$. Furthermore, it is essential to recognize that the internal values of the sphere with a radius $x = 0 \Rightarrow r = l_1$, as established by $r < l_1$, are prohibited, thereby indicating that this region does not form part of the spacetime continuum.

Should one generate a plot of (32), the outcome is represented by Figure 3. It is crucial to note that all graphs are schematic and not to scale, but the key point is that while the electromagnetic field is remarkably strong near the ring singularity, where it diverges to infinity, the navigation through the WH is still possible near to along the polar axis. The singularity residing within the forbidden inner region corresponding to the sphere with radius $r = l_1$.

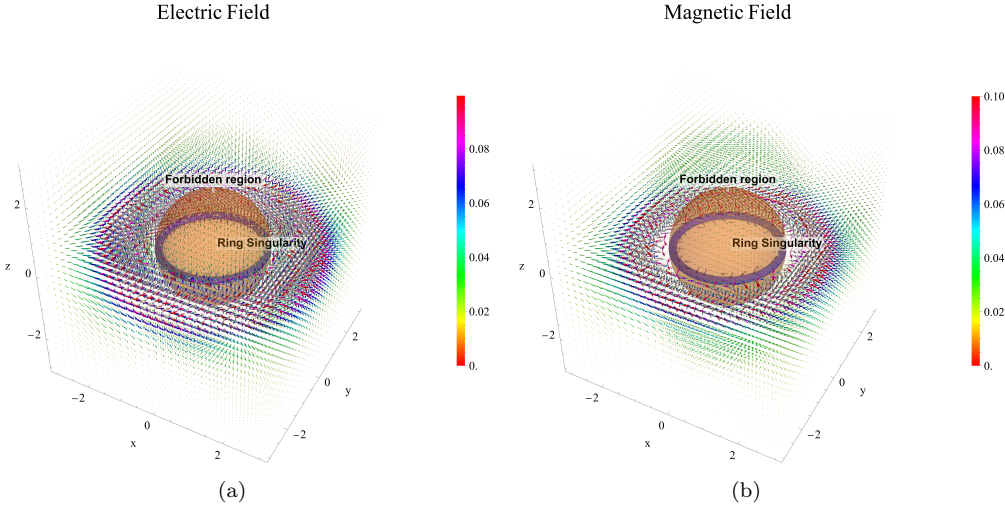


FIG. 3: These illustrations are sourced from [2]. (a) depict the vectorial electric field using pseudo-Cartesian coordinates, and (b) illustrate the vectorial magnetic field. In both images, the ring singularity is represented by a blue torus, while the forbidden region is indicated by a red sphere. These graphs are purely schematic and feature a color intensity scale.

By focusing solely on the magnitude of the electromagnetic field, we have proposed a lower bound for the safe size of a wormhole. For a wormhole with mass $M = 10^7 M_\odot$, the maximum intensity of the magnetic field along the polar axis is approximately 1700 Teslas, which is considered relatively safe.

IV. CAUSAL STRUCTURE

To establish the causal framework of this compact object, it is crucial to examine the smoothness and analyticity of (3). For our purposes, it is preferable to employ spheroidal coordinates, as we have identified the singularity and (11) is available in these coordinates.

In the second class of solutions, as noted in (5), the metric function f remains constant, which implies a priori the absence of event horizons. Taking into account (12b) and (13b) suggest that these expressions preserve regularity for all $y \neq 0$ with $x = 0$. Consequently, the metric remains regular at the throat ($x = 0$) for all $y_0 \neq 0$ and is asymptotically flat.

By utilizing the existence of axial symmetry, the causal structure can be examined using only a subspace (t, x, y) (for further details, see [5]), i.e., fixing $\varphi = \varphi_0$, and $f_0 = 1$ in (11), we obtain

$$ds^2 = -fc^2dt^2 + f^{-1}e^{2k}(d\rho^2 + dz^2) = fc^2dt^2 + \frac{e^{2k}}{f}L^2(x^2 + y^2) \left(\frac{dx^2}{x^2 + 1} + \frac{dy^2}{1 - y^2} \right), \quad (33)$$

Considering $y = y_0$ for simplicity, and defining the total variable as $fdl^2 = e^{2k}(d\rho^2 + dz^2)/f$, we can employ the radial null variables $u = t - l$, $v = t + l$. Consequently, the metric (33) is transformed to $ds^2 = -fdudv$, where $f = f_0$, then a regular metric has been obtained, allowing for the process of compactification to proceed.

Consider the compactification given by $u = \tan U = t - l$, and $v = \tan V = t + l$. The line element is subsequently expressed as $ds^2 = -f(\sec U \sec V)^2 dUdV$. By applying the conformal transformation $\Omega \equiv \cos U \cos V$ and defining the variables $V = T + R$ and $U = T - R$, we derive the final form of the metric

$$d\bar{s}^2 = \Omega^{-2}ds^2 = -f(dT^2 - dR^2). \quad (34)$$

The boundaries in $\Omega = 0$ correspond to the infinite future/past of the space and the time

$$\begin{aligned} u \rightarrow \pm\infty \quad \text{or} \quad U = \pm\pi/2 & \quad \text{implies} \quad T = \pm\pi/2 + R, \\ v \rightarrow \pm\infty \quad \text{or} \quad V = \pm\pi/2 & \quad \text{implies} \quad T = \pm\pi/2 - R, \end{aligned}$$

Through meticulous analysis (the complete process and explanation are given in [3]), one can derive the behaviour close to the singularity as follows:

$$\begin{aligned} R(y_0, x = 0) & \equiv R_G \neq 0, & (35) \\ \lim_{y_0 \rightarrow 0} R(y_0, x = 0) & = \lim_{y_0 \rightarrow 0} R_G = 0, & (36) \end{aligned}$$

and $T \in [-\pi/2, \pi/2]$. In other words, in the equatorial plane, the throat is closed ($R_G(0, 0) = 0$).

Employing the constructed compactification, we have devised Figure 4, which corresponds to the Carter–Penrose diagram for the WH (11). The diagram comprises three distinct regions: the left-hand side depicted in green represents Universe 1, and the region in yellow denotes Universe 2. Both regions have a future time-like infinity (i_+) and a past time-like infinity (i_-), with their respective spatial infinities, j_0 and i_0 , for Universes 1 and 2. Additionally, past and future null infinities ($\mathcal{S}_{1,2}^\pm$) are present for both universes. The third region, illustrated in blue, is the prohibited region, indicating values of $r < l_1$ and hiding the ring singularity. A purple line delineates the geodesic of a particle with speed $c/2$, illustrating its traversal through the wormhole from one universe to the other.

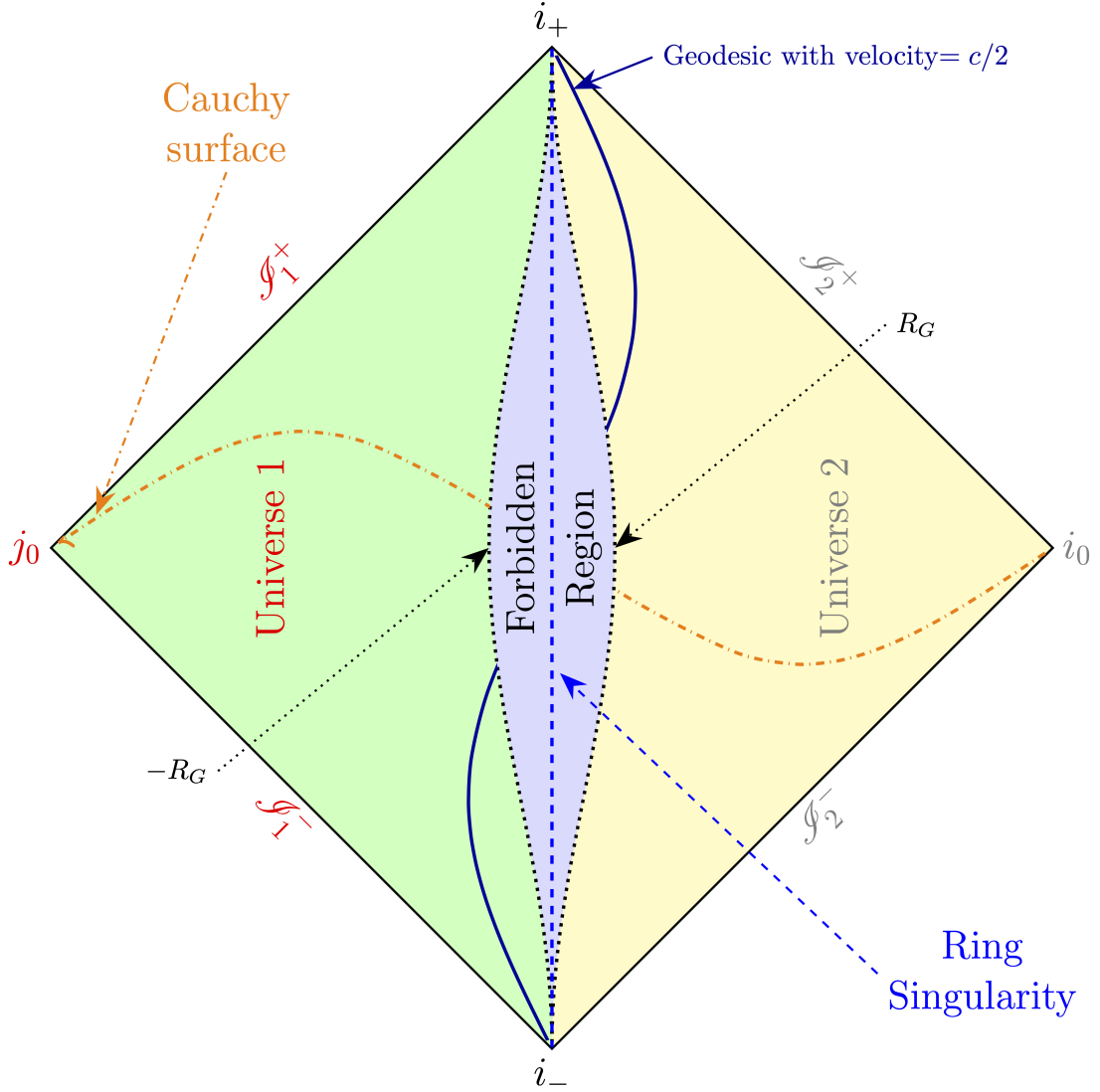


FIG. 4: This illustration is sourced from [3]. The green area represents the Carter-Penrose diagram of one universe, while the yellow area pertains to another. The dotted black lines, which are topologically identified, form the throat in both universes. The dashed blue line depicts the ring singularity, and the orange dotted-dashed line represents a Cauchy surface.

In Boyer-Linquist coordinates, the throat is a \mathbb{S}^2 sphere with a radius of $r = l_1$ and the singularity is in $(r = l_1, \theta = \pi/2)$. The \mathbb{S}^2 sphere of radius $r = l_1$ is topologically connected to another \mathbb{S}^2 sphere of radius $r = -l_1 \quad \forall \theta$. In Weyl-coordinates, the throat is at $z = 0$, and the $z = 0^+$ plane is topologically identified as $z = 0^-$, in this case, the ring singularity is in $(\rho = L, z = 0)$. The black dotted lines represent the throat ($\pm R_G$), which is topologically identified and corresponds to the aforementioned descriptions.

It is now understood that the throat *dresses* the ring singularity similarly to how event horizons hide singularities in black holes. The mechanics are as follows: when one attempts to approach the singularity in the equatorial plane, the wormhole tends to constrict its throat. Consequently, the compact objects prevent traversal to another universe. Moreover, according to $\theta \neq \phi/2$, this will never pose a problem, because as we approach the ring singularity, we first encounter the throat, which consequently transports us into another universe.

Using the definitions of Killing horizons, Cauchy horizons, and event horizons as provided in reference [5], we can examine the solution (11).

We commence our analysis on the absence of event horizons. In order to discern the event horizons within these solutions, we shall employ the Killing vector $K_t = \partial_t + \Omega \partial_\psi$, where Ω is constant over the horizon \mathcal{H} . This will be achieved by computing the norm of the said vector K_t :

$$\begin{aligned} g(K_t, K_t) &= g_{tt} + 2\Omega g_{t\psi} + \Omega^2 g_{\psi\psi} = 0, \\ \Rightarrow \Omega_{\pm} &= -\frac{g_{t\psi}}{g_{\psi\psi}} \pm \frac{\sqrt{-(g_{\psi\psi}g_{tt} - (g_{t\psi})^2)}}{g_{\psi\psi}}, \end{aligned}$$

Consequently, the event horizon can be determined \mathcal{H} provided that Ω are non-degenerate and remain constant.

$$g_{\psi\psi}g_{tt} - (g_{t\psi})^2 = -\rho = -L\sqrt{(x^2 + 1)(1 - y^2)} = 0, \quad (37a)$$

$$\Omega = \Omega_- = \Omega_+ = -\frac{g_{t\psi}}{g_{\psi\psi}} = -(\omega|_{\mathcal{H}})^{-1} \quad (37b)$$

The sole feasible event horizon is located in the polar axis $y = \pm 1$, characterized by $\omega|_{\mathcal{H}} = -L\tau_0$. However, upon opting for the asymptotically flat solution $\tau_0 = 0$, the apparent event horizon vanishes.

A null hyper-surface $G(x, y)$ is defined by the existence of a normal vector ζ , which adheres to the condition $\zeta^2 = 0$ over the hyper-surface. Thus, a Killing horizon is characterized as a null hypersurface that contains a Killing vector ξ , which is concurrently null $\xi^2 = 0$ and tangent $\xi^\mu \zeta_\mu = 0$ throughout $G(x, y)$. Let

$$G(x, y) \equiv \rho^2 - \omega^2 = 0 \quad \text{implies} \quad \omega|_G = \pm\rho, \quad (38)$$

then, the normal vector is

$$\zeta \equiv (g^{xx}\partial_x G)\partial_x + (g^{yy}\partial_y G)\partial_y = e^{-2k}(\partial_x G\partial_x + \partial_y G\partial_y), \quad (39)$$

where condition $\zeta^2|_G = 0$ is satisfied. Selecting the killing vector $\xi = \partial_\varphi$, and computing

$$\xi^2|_G = g(\partial_\varphi, \partial_\varphi)|_G = g_{\varphi\varphi}|_G = \rho^2 - \omega^2|_G = 0, \quad \xi^\mu \zeta_\mu = 0. \quad (40)$$

It is observable that $\xi \propto \zeta$, indicating that ξ acts as both the normal and tangent vector to the hypersurface $\omega = \pm\rho$. It is crucial to clarify that this horizon signifies the boundary at which causality violation, **it is not a event horizon**.

The surface gravity is provided by $\nabla_\mu(\xi^2)|_G = -2\varrho\xi_\mu$, and employing the one-form Killing vector $\xi^\sharp = g_{t\varphi}dt + g_{\varphi\varphi}d\varphi$, it is possible to determine

$$\begin{aligned} d(\xi^2) &= d(g_{\varphi\varphi}) = (\partial_x g_{\varphi\varphi})dx + (\partial_y g_{\varphi\varphi})dy, \\ &= 2(\omega\partial_x\omega - \rho\partial_x\rho)dx + 2(\omega\partial_y\omega - \rho\partial_y\rho)dy. \end{aligned} \quad (41)$$

Therefore $d(\xi^2)|_G = 0 \Rightarrow \varrho = 0$, indicating zero surface gravity at this Killing horizon, allowing an observer at infinity to cross it easily.

Now, taking advantage of the norm of the Killing vector ∂_φ , we can see some important things

- The Killing vector $K_\varphi = \partial_\varphi$ is space-like if and only if $g(K_\varphi, K_\varphi) = g_{\varphi\varphi} = \rho^2 - \omega^2 \geq 0$.
- t is a temporal-type function if and only if $g(\nabla t, \nabla t) = g(g^{t\nu}\partial_\nu, g^{t\mu}\partial_\mu) = g^{t\nu}g^{t\mu}g_{\mu\nu} = -(\rho^2 - \omega^2)/\rho^2 < 0$, then $\rho^2 - \omega^2 > 0$.

Based on the aforementioned evidence and the analysis provided in [18], it can be ascertained that the *Closed Time-like Curves* (CTC) manifest under the condition $g_{\phi\phi} = \rho^2 - \omega^2 < 0$ in the context of our specific study.

After conducting some analysis, it is evident that $\rho^2 > g_{\phi\phi} = \rho^2 - \omega^2 \quad \forall \{x, y\}$. Consequently, before an entity can interact with points where CTCs manifest, the entity traverses the wormhole into another universe. A similar phenomenon occurs with the Kerr–Newman black hole, where a ring singularity exists, and CTCs emerge nearby. However, the event horizon conceals this occurrence, enabling us to apply the solution to the exterior regions, outside the event horizon. In our scenario, the throat regulates the solution, and we consider the entire object because the throat is closed in the equatorial plane. Before an object can approach the singularity or CTCs appear, it passes through the wormhole.

V. FLAT SUBSPACES METHOD

In this section, we will briefly describe a method for solving the vacuum Einstein field equations (EFEs) in higher dimensions.

In [36], the authors consider a spacetime with a metric \hat{g} , which admits n commutative Killing vectors. Under this assumption, the metric \hat{g} can be written as

$$\hat{g} = f(v, \zeta)(dv^2 + d\zeta^2) + g_{ij}(v, \zeta)dx^i dx^j \quad (42)$$

for all $i, j \in \{3, \dots, n+2\}$. In a vacuum, the Einstein field equations are equivalent to $R_{AB} = 0$ for all $A, B \in \{1, \dots, n+2\}$. Then,

$$(vg_{,w}g^{-1})_{,\bar{w}} + (vg_{,\bar{w}}g^{-1})_{,w} = 0, \quad (43)$$

$$(\ln f v^{1-1/n})_{,W} = \frac{1}{2}v \operatorname{tr}(g_{,w}g^{-1})^2 \text{ for } W \in \{w, \bar{w}\}, \quad (44)$$

where g is defined as $(g)_{ij} = -v^{-2/n}g_{ij}$, $v = \sqrt{-\det g_{ij}}$ and $w = v + i\zeta$. Note that g is a symmetry matrix and belongs to the Lie group $SL(n, \mathbb{R})$.

In order to solve the chiral Equation (43), they assume that g depends on a set of parameters $\{\xi^a(w, \bar{w})\}$, which satisfy the generalized Laplace equation

$$(v\xi_{,w}^a)_{,\bar{w}} + (v\xi_{,\bar{w}}^a)_{,w} = 0. \quad (45)$$

Then, the chiral Equation (43) becomes

$$A_{a,b} + A_{b,a} = 0 \text{ for all } a, b \in \{1, \dots, r\}, \quad (46)$$

where $A_a = g_{,a}g^{-1}$ and $r \in \{1, \dots, n\}$. The partial derivative of A_a with respect to ξ^b is given by $A_{a,b} = -\frac{1}{2}[A_a, A_b]$. They suppose that the matrices A_a are constant. Consequently, $\{A_a\}$ is a set of pairwise commuting matrices.

Since the determinant of g is constant, the matrices A_a are traceless; hence, they belong to the Lie algebra $\mathfrak{sl}(n, \mathbb{R})$. The matrices A_a are transformed as $A_a \rightarrow \mathfrak{C}A_a\mathfrak{C}^{-1}$ when $g \rightarrow \mathfrak{C}g\mathfrak{C}^T$ with constant $\mathfrak{C} \in SL(n, \mathbb{R})$. Thus, we can define an equivalence relation under this transformation and partition the set $\{A_a\}$ into equivalence classes. In [35], a classification of the equivalence classes of $\mathfrak{sl}(n, \mathbb{R})$ is given, which is based on their types of eigenvalues.

In [36], the authors assume that A_1 is representative of some equivalence classes of $\mathfrak{sl}(n, \mathbb{R})$. Then, A_2 is chosen from the centralizer of A_1 , i.e., $\mathcal{C}(A_1)$, and so on, until A_r is chosen from $\mathcal{C}(\{A_1, \dots, A_{r-1}\})$. Since computing the centralizer of large and complex matrices is difficult, the same authors propose an alternative. They demonstrate that there exists a commutative algebra \mathfrak{A} of dimension n contained in the centralizer of a representative of some equivalence classes of $\mathfrak{sl}(n, \mathbb{R})$. In this way, $\{A_a\}$ is a subset in \mathfrak{A} . Hence, the matrices A_a are selected from \mathfrak{A} . Furthermore, they compute the centralizers of the equivalence classes of $\mathfrak{sl}(n, \mathbb{R})$ and determine the commutative algebras contained in them.

Let $\{A_a\} \subset \mathfrak{sl}(n, \mathbb{R})$ be a set of pairwise commuting matrices, and let $\{\xi^a(w, \bar{w})\}$ be a set of solutions to the generalized Laplace equation. Then, the solution $g(w, \bar{w})$ is given by

$$g(w, \bar{w}) = \exp(\xi^a(w, \bar{w})A_a)g_0, \quad (47)$$

where $g_0 \in \mathcal{I}(\{A_a\}) = \{M \in \mathbf{Sym}_n : A_a M = M A_a^T \text{ for all } a \in \{1, \dots, r\}\}$. Now, Equation (44) can be expressed in terms of the matrices A_a and the parameters $\xi^a(w, \bar{w})$ as

$$(\ln f v^{1-1/n})_{,W} = \frac{\operatorname{tr} A_a A_b}{2} v \xi_{,W}^a \xi_{,W}^b. \quad (48)$$

The solutions of chiral equations given by $g(w, \bar{w}) = \exp(\xi(w, \bar{w})A)g_0$ can be found in [35].

VI. A FAMILY OF WORMHOLES IN 5D

In this section, we will build an exact solution to the 5-dimensional EFE using the method introduced in the previous section and the mathematical tools from [36].

Let

$$A_1 = \begin{bmatrix} 1 & & \\ & 1 & \\ & & -2 \end{bmatrix} \text{ and } A_2 = \begin{bmatrix} & -1 & \\ 1 & & \\ & & 0 \end{bmatrix} \quad (49)$$

be a pair of pairwise commuting matrices in $\mathfrak{sl}(3, \mathbb{R})$. Let

$$\xi^1 = \xi_0^1 - \frac{2}{3} \ln v + q \tan^{-1} \frac{r}{r_0} \text{ and } \xi^2 = \xi_0^2 + p \tan^{-1} \frac{r}{r_0} \quad (50)$$

be a pair of solutions to the generalized Laplace equation

$$((r^2 + r_0^2)\xi_{,r}^a)_{,r} + \frac{1}{\sin \theta} (\xi_{,\theta}^a \sin \theta)_{,\theta} = 0, \quad (51)$$

which is written in terms of the Boyer–Lindquist coordinates as follows:

$$v = \sqrt{r^2 + r_0^2} \sin \theta \text{ and } \zeta = r \cos \theta, \quad (52)$$

where $r \geq 0$, $0 \leq \theta \leq \pi$, r_0 is a positive number, p is a natural number, and q, ξ_0^1, ξ_0^2 are real numbers. Since g_0 is a constant matrix in $\mathcal{I}(\{A_1, A_2\})$, then it has the form

$$g_0 = -\text{diag} \left[\begin{bmatrix} C_t & D \\ D & -C_t \end{bmatrix}, C_\phi \right], \quad (53)$$

where $C_t, D, C_\phi \in \mathbb{R}$ are constants. To build a solution to the chiral equation, we compute Equation (47). Therefore,

$$g(r, \theta) = -\rho^{-\frac{2}{3}} \text{diag} \left[\Xi \begin{bmatrix} \mathcal{U}_p\left(\frac{r}{r_0}\right) & \mathcal{V}_p\left(\frac{r}{r_0}\right) \\ \mathcal{V}_p\left(\frac{r}{r_0}\right) & -\mathcal{U}_p\left(\frac{r}{r_0}\right) \end{bmatrix}, \frac{\rho^2 \Xi^{-2}}{\mu^2 + \nu^2} \right], \quad (54)$$

where

$$\Xi = \frac{\exp\left(q \tan^{-1} \frac{r}{r_0}\right)}{\exp\left(q \frac{\pi}{2}\right)}, \quad (55)$$

$$\mathcal{U}_p(x) = \mu T_p\left(\frac{1}{\sqrt{x^2 + 1}}\right) - \frac{\nu x}{\sqrt{x^2 + 1}} U_{p-1}\left(\frac{1}{\sqrt{x^2 + 1}}\right), \quad (56)$$

$$\mathcal{V}_p(x) = \nu T_p\left(\frac{1}{\sqrt{x^2 + 1}}\right) + \frac{\mu x}{\sqrt{x^2 + 1}} U_{p-1}\left(\frac{1}{\sqrt{x^2 + 1}}\right) \quad (57)$$

for all $x \in \mathbb{R}$, $\mu = C_t \cos \xi_0^2 - D \sin \xi_0^2$, $\nu = D \cos \xi_0^2 + C_t \sin \xi_0^2$, T_p and U_{p-1} are Chebyshev polynomials of the first and second kind, respectively.

In what follows, we present some properties of the functions \mathcal{U}_p and \mathcal{V}_p .

- Recurrence relations.

$$\begin{cases} \mathcal{U}_p(x) = \frac{2}{\sqrt{x^2 + 1}} \mathcal{U}_{p-1}(x) - \mathcal{U}_{p-2}(x), \\ \mathcal{V}_p(x) = \frac{2}{\sqrt{x^2 + 1}} \mathcal{V}_{p-1}(x) - \mathcal{V}_{p-2}(x), \end{cases} \quad (p > 2). \quad (58)$$

- Pythagorean relation.

$$\mathcal{U}_p^2(x) + \mathcal{V}_p^2(x) = \mu^2 + \nu^2. \quad (59)$$

- Roots.

$$\begin{aligned} x_k &= \tan\left(\frac{\tan^{-1}(\mu/\nu) + k\pi}{p}\right) && \text{for } \mathcal{U}_p, \\ x_k &= \tan\left(\frac{-\tan^{-1}(\nu/\mu) + k\pi}{p}\right) && \text{for } \mathcal{V}_p, \end{aligned} \quad \text{where } k \in \{0, \dots, p-1\}. \quad (60)$$

- Limits.

$$\begin{aligned} \lim_{x \rightarrow \pm\infty} \mathcal{U}_p(x) &= (-)^{\frac{p}{2}} \mu, & \lim_{x \rightarrow \pm\infty} \mathcal{V}_p(x) &= (-)^{\frac{p}{2}} \nu & \text{for } p \text{ even,} \\ \lim_{x \rightarrow \pm\infty} \mathcal{U}_p(x) &= \mp (-)^{\frac{p-1}{2}} \nu, & \lim_{x \rightarrow \pm\infty} \mathcal{V}_p(x) &= \pm (-)^{\frac{p-1}{2}} \mu & \text{for } p \text{ odd.} \end{aligned} \quad (61)$$

- Differentiation.

$$\frac{d\mathcal{U}_p}{dx}(x) = \frac{-p}{x^2+1} \mathcal{V}_p(x), \quad \frac{d\mathcal{V}_p}{dx}(x) = \frac{p}{x^2+1} \mathcal{U}_p(x). \quad (62)$$

Solving the partial differential equations

$$\begin{aligned} \left(\ln f \nu^{1-1/n} \right)_{,r} &= \frac{\text{tr } A_a A_b}{4} \frac{r \sin^2 \theta}{\Delta} \left[\xi_{,r}^a \xi_{,r}^b + \frac{2 \cot \theta \xi_{,r}^a \xi_{,\theta}^b}{r} - \frac{\xi_{,\theta}^a \xi_{,\theta}^b}{r^2 + r_0^2} \right], \\ \left(\ln f \nu^{1-1/n} \right)_{,\theta} &= -\frac{\text{tr } A_a A_b}{4} \frac{\sin \theta \cos \theta}{\Delta} \left[\xi_{,r}^a \xi_{,r}^b - \frac{2r \tan \theta \xi_{,r}^a \xi_{,\theta}^b}{r^2 + r_0^2} - \frac{\xi_{,\theta}^a \xi_{,\theta}^b}{r^2 + r_0^2} \right], \end{aligned} \quad (63)$$

we find

$$f(r, \theta) = \Delta^{\frac{3q^2 - p^2}{4}} \Xi^{-2}, \quad (64)$$

where

$$\Delta = \frac{r^2 + r_0^2 \cos^2 \theta}{r^2 + r_0^2}. \quad (65)$$

Therefore, an exact solution is

$$\begin{aligned} \hat{g}_p &= -\mathcal{U}_p(r/r_0) \Xi dt^2 + \frac{\Delta^l (dr^2 + (r^2 + r_0^2) d\theta^2) + (r^2 + r_0^2) \sin^2 \theta d\phi^2}{\Xi^2} \\ &\quad + \mathcal{U}_p(r/r_0) \Xi d\psi^2 + 2\mathcal{V}_p(r/r_0) \Xi dt d\psi \end{aligned} \quad (66)$$

where $l = 1 + \frac{3}{4}q^2 - \frac{1}{4}p^2$ and ψ is the coordinate of the fifth dimension. In the limit $r \rightarrow \infty$, if $\mathcal{U}_p(r/r_0) \rightarrow 1$ and $\mathcal{V}_p(r/r_0) \rightarrow 0$, then $\hat{g}_p \rightarrow -dt^2 + dr^2 + r^2 d\Omega_2^2 + d\psi^2$, where $d\Omega_2^2 = d\theta^2 + \sin^2 \theta d\phi^2$.

For the metric (66) to describe a wormhole, we extend the values of r ; that is, $r \in \mathbb{R}$. However, we reject the odd values of p , because $\mathcal{U}_p(r/r_0) \rightarrow -1$ as $r \rightarrow -\infty$. This means that t and ψ are spatial and temporal coordinates, respectively, at infinity. When $\mu = -1$, $\nu = 0$ and $q = 0$, the metric \hat{g}_2 is

$$\hat{g}_2 = \frac{r^2 - r_0^2}{r^2 + r_0^2} (d\psi^2 - dt^2) + dr^2 + (r^2 + r_0^2) d\Omega_2^2 - \frac{4r_0 r}{r^2 + r_0^2} dt d\psi, \quad (67)$$

which describes a wormhole [9, 21]. For this metric, the Kretschmann invariant is

$$R_{ABCD} R^{ABCD} = 24 \frac{(r_0^2 - 2r^2) r_0^2}{(r^2 + r_0^2)^4}. \quad (68)$$

VII. CONCLUSIONS

The second family of solutions function as wormholes, and it is crucial to note that the throat of the wormhole hides all the potential irregularities that may exist in the flat solution. In this compact object, there is an absence of event horizons and ergo-regions, yet closed time-like curves (CTCs) do appear within the blue region of Figure 4. Essentially, one traverses the wormhole prior to encountering the singularity or the causal violation region. The wormhole described herein adheres to the null energy condition (NEC) in the context of a dilaton scalar field and possesses a ring singularity without necessitating asymptotic flatness. We suggest specific bounds to guarantee the stability and safety of the wormhole.

In Section V, we briefly explain the flat subspaces method, which allows us to build exact solutions to the vacuum EFE in higher dimensions. Its main advantage over other methods lies in the use of algebraic techniques. In this approach, an exact solution to the EFE is derived from the solution to the chiral equation. Specifically, it only requires

a set $\{A_a\}$ of pairwise commuting matrices, a set $\{\xi^a(w, \bar{w})\}$ of solutions to the generalized Laplace equation and a constant matrix $g_0 \in \mathcal{I}(\{A_a\})$ to compute a solution of the chiral equation. In Section VI, we built a family of wormholes in five dimensions. However, only metric \hat{g}_2 , given by Equation (67), was studied in detail. Currently, we study the other values of p .

All authors have contributed equally to the conception, analysis, and preparation of this work.

This work was also partially supported by SECIHTI México under grants A1-S-8742, 304001, 376127, 240512.

The authors declare that there are no conflicts of interest.

Appendix A

Parameter

Constraint Equation

For obtain the parameter constrain we will use the metric

$$ds^2 = -f(d(ct) - \omega d\varphi)^2 + f^{-1} \left(L^2(x^2 + 1)(1 - y^2)d\varphi^2 + L^2(x^2 + y^2)e^{2k} \left\{ \frac{dx^2}{x^2 + 1} + \frac{dy^2}{1 - y^2} \right\} \right),$$

where the function metrics associated to the solution (10) are

$$\begin{aligned} f &= f_0 = 1, \\ \omega &= \frac{L}{f_0} \left(\frac{\lambda_0 x(1 - y^2) - \tau_0 y(x^2 + 1)}{x^2 + y^2} \right), \\ A_\varphi &= \frac{\sqrt{f_0}}{2\kappa_0 \sqrt{\sigma_0}} \left(A_3 - \frac{\omega}{L} e^{-\lambda_c} \right), \\ A_t &= \frac{\sqrt{f_0}}{2\kappa_0 \sqrt{\sigma_0}} \left(e^{-\lambda_c} - 1 \right), \\ k_c &= k_{\lambda_5} + k_{\lambda_6} - k_0 \frac{8xy(1 - y^2)(x^2 + 1)(x^2 - y^2)\lambda_0\tau_0}{4(x^2 + y^2)^4}, \end{aligned}$$

and the 4-potential $A_\mu = [A_t(\rho, z), 0, 0, A_\varphi(\rho, z)]$.

By applying the variable transformation (See the articles [24–26]) $\kappa^2 = e^{-2\alpha_0 \phi}$ and considering the scalar field potential described in Equation (5), we find that

$$\phi = -\frac{\ln \kappa}{\alpha_0} = -\frac{\lambda}{\alpha_0} \quad | \quad \kappa_0 = 1.$$

Next, by applying the Einstein Field Equations presented as follows

$$[EE]_{\mu\nu} \equiv R_{\mu\nu} - 2\epsilon_0 \nabla_\mu \phi \nabla_\nu \phi - 2\sigma_0 e^{-2\alpha_0 \phi} \left(F_{\mu\sigma} F_\nu{}^\sigma - \frac{1}{4} g_{\mu\nu} F^2 \right),$$

with $F_{\mu\nu} = \partial_\mu A_\nu - \partial_\nu A_\mu$, and $F^2 = F^{\mu\nu} F_{\mu\nu}$, we can replace the previously mentioned solution related to λ_c , resulting in

$$[EE]_{\mu\nu} = \begin{pmatrix} 0 & 0 & 0 & 0 \\ 0 & [EE]_{xx} & [EE]_{xy} & 0 \\ 0 & [EE]_{yx} & [EE]_{yy} & 0 \\ 0 & 0 & 0 & 0 \end{pmatrix} = 0, \quad (\text{A2})$$

where

$$[EE]_{xx} = \frac{(\alpha_0^2(4k_0 + 1) - 4\epsilon_0) (2\lambda_0 xy + \tau_0 (x^2 - y^2))^2}{2\alpha_0^2 (x^2 + y^2)^4} = 0, \quad (\text{A3a})$$

$$[EE]_{yy} = \frac{(\alpha_0^2(4k_0 + 1) - 4\epsilon_0) (\lambda_0 (y^2 - x^2) + 2\tau_0 xy)^2}{2\alpha_0^2 (x^2 + y^2)^4} = 0, \quad (\text{A3b})$$

$$[EE]_{xy} = [EE]_{yx} = -\frac{(\alpha_0^2(4k_0 + 1) - 4\epsilon_0)}{2\alpha_0^2 (x^2 + y^2)^4} \left(2\lambda_0^2 xy (x^2 - y^2) + \lambda_0 \tau_0 (-6x^2 y^2 + x^4 + y^4) + 2\tau_0^2 xy (y^2 - x^2) \right) = 0, \quad (\text{A3c})$$

Therefore, (A3) is fulfilled if and only if

$$(\alpha_0^2(4k_0 + 1) - 4\epsilon_0) = 0.$$

The *Maxwell Equation* (2a) and the *Klein–Gordon Equation* (2b) are satisfied regardless of the constraints on this parameter.

-
- [1] Bixano, L., Matos, T., 2025a. Einstein–Maxwell–dilaton wormholes that meet the energy conditions. *Phys. Rev. D* 111, 084056. doi:doi:10.1103/PhysRevD.111.084056, [arXiv:2502.07206](#).
- [2] Bixano, L., Matos, T., 2025b. On the Possibility of the Existence of Wormholes in Nature [arXiv:2505.20167](#).
- [3] Bixano, L., Matos, T., 2025c. The space-time structure of an untouchable naked singularity [arXiv:2508.01820](#).
- [4] Bronnikov, K.A., 1973. Scalar-tensor theory and scalar charge. *Acta Phys. Polon. B* 4, 251–266.
- [5] Chrusciel, P., 2023. *Geometry of Black Holes*. International Series of Monographs on Physics, Oxford University Press.
- [6] Del Águila, J.C., Matos, T., 2019. Wormhole Cosmic Censorship: An Analytical Proof. *Class. Quant. Grav.* 36, 015018. doi:doi:10.1088/1361-6382/aaf336, [arXiv:1806.03747](#).
- [7] Del Águila, J.C., Matos, T., 2023. Geodesic completeness of a ring wormhole. *Phys. Rev. D* 107, 064047. doi:doi:10.1103/PhysRevD.107.064047, [arXiv:2303.12251](#).
- [8] Del Águila, J.C., Matos, T., Miranda, G., 2019. Exact Rotating Magnetic Traversable Wormholes satisfying the Energy Conditions. *Phys. Rev. D* 99, 124045. doi:doi:10.1103/PhysRevD.99.124045, [arXiv:1507.02348](#).
- [9] Dzhunushaliev, V.D., 1998. Multidimensional geometrical model of the renormalized electrical charge with splitting off the extra coordinates. *Mod. Phys. Lett. A* 13, 2179–2186. doi:doi:10.1142/S021773239800231X, [arXiv:gr-qc/9807080](#).
- [10] Ellis, H.G., 1973. Ether flow through a drainhole - a particle model in general relativity. *J. Math. Phys.* 14, 104–118. doi:doi:10.1063/1.1666161.
- [11] Gao, P., Jafferis, D.L., Wall, A.C., 2017. Traversable Wormholes via a Double Trace Deformation. *JHEP* 12, 151. doi:doi:10.1007/JHEP12(2017)151, [arXiv:1608.05687](#).
- [12] Goulart, P., 2018. Phantom wormholes in Einstein–Maxwell–dilaton theory. *Class. Quant. Grav.* 35, 025012. doi:doi:10.1088/1361-6382/aa9dfc, [arXiv:1708.00935](#).
- [13] Hawking, S., 1966a. The Occurrence of singularities in cosmology. *Proc. Roy. Soc. Lond. A* 294, 511–521. doi:doi:10.1098/rspa.1966.0221.
- [14] Hawking, S., 1966b. The Occurrence of singularities in cosmology. II. *Proc. Roy. Soc. Lond. A* 295, 490–493. doi:doi:10.1098/rspa.1966.0255.
- [15] Hawking, S., 1967. The occurrence of singularities in cosmology. III. Causality and singularities. *Proc. Roy. Soc. Lond. A* 300, 187–201. doi:doi:10.1098/rspa.1967.0164.
- [16] Hawking, S.W., Ellis, G.F.R., 2023. *The Large Scale Structure of Space-Time*. Cambridge Monographs on Mathematical Physics, Cambridge University Press. doi:doi:10.1017/9781009253161.
- [17] Lazov, B., Nedkova, P., Yazadjiev, S., 2018. Uniqueness theorem for static phantom wormholes in Einstein–Maxwell–dilaton theory. *Phys. Lett. B* 778, 408–413. doi:doi:10.1016/j.physletb.2018.01.059, [arXiv:1711.00290](#).
- [18] Lobo, F., Crawford, P., 2003. Time, closed time - like curves and causality. *NATO Sci. Ser. II* 95, 289–296. [arXiv:gr-qc/0206078](#).
- [19] Lobo, F.S.N., 2005. Phantom energy traversable wormholes. *Phys. Rev. D* 71, 084011. doi:doi:10.1103/PhysRevD.71.084011, [arXiv:gr-qc/0502099](#).
- [20] Lobo, F.S.N. (Ed.), 2017. *Wormholes, Warp Drives and Energy Conditions*. volume 189 of *Fundamental Theories of Physics*. Springer. doi:doi:10.1007/978-3-319-55182-1, [arXiv:2103.05610](#).
- [21] Lü, H., Mei, J., 2008. Ricci-flat and charged wormholes in five dimensions. *Physics Letters B* 666, 511–516. URL: <https://www.sciencedirect.com/science/article/pii/S0370269308009763>, doi:doi:https://doi.org/10.1016/j.physletb.2008.07.100.
- [22] Maldacena, J., Milekhin, A., Popov, F., 2023. Traversable wormholes in four dimensions. *Class. Quant. Grav.* 40, 155016. doi:doi:10.1088/1361-6382/acde30, [arXiv:1807.04726](#).

- [23] Matos, T., 2010. Class of Einstein-Maxwell Phantom Fields: Rotating and Magnetised Wormholes. *Gen. Rel. Grav.* 42, 1969–1990. doi:doi:10.1007/s10714-010-0976-6, [arXiv:0902.4439](#).
- [24] Matos, T., Miranda, G., Sanchez-Sanchez, R., Wiederhold, P., 2009. Class of Einstein-Maxwell-Dilaton-Axion Space-Times. *Phys. Rev. D* 79, 124016. doi:doi:10.1103/PhysRevD.79.124016, [arXiv:0905.4097](#).
- [25] Matos, T., Nunez, D., Estevez, G., Rios, M., 2000a. Rotating 5-D Kaluza-Klein space-times from invariant transformations. *Gen. Rel. Grav.* 32, 1499–1525. doi:doi:10.1023/A:1001982001694, [arXiv:gr-qc/0001039](#).
- [26] Matos, T., Nunez, D., Rios, M., 2000b. Class of Einstein-Maxwell dilatons, an ansatz for new families of rotating solutions. *Class. Quant. Grav.* 17, 3917–3934. doi:doi:10.1088/0264-9381/17/18/323, [arXiv:gr-qc/0008068](#).
- [27] Matos, T., Urena-Lopez, L.A., Miranda, G., 2016. Wormhole Cosmic Censorship. *Gen. Rel. Grav.* 48, 61. doi:doi:10.1007/s10714-016-2040-7, [arXiv:1203.4801](#).
- [28] Minazzoli, O., 2024. On the Principle of Relativity of Inertia in Both General and Entangled Relativities. *Phys. Part. Nucl.* 55, 1488–1493. doi:doi:10.1134/S1063779624701132, [arXiv:2505.04667](#).
- [29] Minazzoli, O., Wavasseur, M., 2025. Compact objects with scalar charge embedded in a magnetic or electric field in Einstein–Maxwell-dilaton theories. *Eur. Phys. J. C* 85, 474. doi:doi:10.1140/epjc/s10052-025-14179-w, [arXiv:2502.13829](#).
- [30] Minazzoli, O., Wavasseur, M., Chehab, T., 2025. Deriving Entangled Relativity [arXiv:2506.15209](#).
- [31] Morris, M.S., Thorne, K.S., 1988. Wormholes in space-time and their use for interstellar travel: A tool for teaching general relativity. *Am. J. Phys.* 56, 395–412. doi:doi:10.1119/1.15620.
- [32] Penrose, R., 1965. Gravitational collapse and space-time singularities. *Phys. Rev. Lett.* 14, 57–59. doi:doi:10.1103/PhysRevLett.14.57.
- [33] Penrose, R., 1969. Gravitational collapse: The role of general relativity. *Riv. Nuovo Cim.* 1, 252–276. doi:doi:10.1023/A:1016578408204.
- [34] Poisson, E., Visser, M., 1995. Thin shell wormholes: Linearization stability. *Phys. Rev. D* 52, 7318–7321. doi:doi:10.1103/PhysRevD.52.7318, [arXiv:gr-qc/9506083](#).
- [35] Sarmiento-Alvarado, I.A., Wiederhold, P., Matos, T., 2023. One-dimensional subspaces of the $SL(n, \mathbb{R})$ chiral equations. *International Journal of Theoretical Physics* 62, 270. doi:doi:10.1007/s10773-023-05520-8.
- [36] Sarmiento-Alvarado, I.A., Wiederhold, P., Matos, T., 2025. Flat subspaces of the $SL(n, \mathbb{R})$ chiral equations. *General Relativity and Gravitation* 57, 132. doi:doi:10.1007/s10714-025-03467-1.
- [37] Visser, M., 1996. *Lorentzian Wormholes: From Einstein to Hawking*. American Institute of Physics Melville, NY.